Ecological Indicators 60 (2016) 503–513

Contents lists available at ScienceDirect

Ecological Indicators

journal homepage: www.elsevier.com/locate/ecolind

Applying remote sensing techniques to monitoring seasonal and interannual changes of aquatic vegetation in Taihu Lake, China

Juhua Luo[a,*], Xinchuan Li[b], Ronghua Ma[a,*], Fei Li[a], Hongtao Duan[a], Weiping Hu[a], Boqiang Qin[a], Wenjiang Huang[c]

[a] Key Laboratory of Watershed Geographic Sciences, Nanjing Institute of Geography and Limnology, Chinese Academy of Sciences, Nanjing 210008, China
[b] School of Earth Sciences and Engineering, Hohai University, Nanjing 210098, China
[c] Key Laboratory of Digital Earth Sciences, Institute of Remote Sensing and Digital Earth, Chinese Academy of Sciences, Beijing 100094, China

ARTICLE INFO

Article history:
Received 6 March 2015
Received in revised form 28 June 2015
Accepted 28 July 2015
Available online 15 August 2015

Keywords:
Wetland
Remote sensing
Aquatic vegetation
Classification tree
Taihu Lake

ABSTRACT

Knowledge of the composition and areal distribution of aquatic vegetation types, as well as their seasonal and interannual variations, is crucial for managing and maintaining the balance of lake ecosystems. In this study, a series of remotely sensed images with a resolution of 30 m (HJ-CCD and Landsat TM) were collected and used to map the distribution of aquatic vegetation types in Taihu Lake, China. Seasonal and interannual dynamics of aquatic vegetation types were explored and analyzed. The distribution areas of Type I (emergent, floating-leaved and floating vegetation) and Type II (submerged vegetation) were used to model their growing season phenology by double logistic functions. The resulting double logistic models showed, the area of Type I reached its peak in mid-August, and the maximum area for Type II occurred in mid-September. From 1984 to 2013, Type I area increased continuously from 59.75 km^2 to 148.00 km^2 (R^2 = 0.84), whereas the area covered by Type II first increased and then decreased, with a trend conforming to a significant quadratic curve (R^2 = 0.83). The eutrophication and stable state of Taihu Lake was assessed using a simple indicator which was expressed as a ratio of Type II area to Type I area. The results showed that the eutrophication in the lake might have been increasing in the area studied since 2000. Additionally, the results showed that air temperature had likely a direct effect on the growth of Type I (R^2 = 0.66) and a significant, but delayed, effect on the growth of Type II.

1. Introduction

Aquatic macrophytes are important for primary production and environmental protection in shallow lakes and provide multiple ecological functions (Barko et al., 1991; Carpenter and Lodge, 1986; Gumbricht, 1993; Hu et al., 2010; Li and Yang, 1995), such as stabilizing sediments, slowing water currents, purifying water and maintaining fishery production. Studies have indicated that aquatic vegetation, especially submerged macrophytes, can cause aquatic ecosystems to shift from a turbid algae-dominated state to a clear-water plant-dominated state (Folke et al., 2004; Soana et al., 2012). However, an excessive amount of macrophytes, especially floating-leaved vegetation, may cause an adverse shift in shallow lakes from a clear-water plant-dominated state to a turbid algae-dominated state (Zhao et al., 2013). Therefore, to effectively manage shallow lakes, it is very important to monitor the distribution and variations of aquatic macrophytes and to understand their community structures.

Across a lake with an area of thousands of square kilometers, such as the Taihu Lake, it is laborious and difficult to survey the types and distributions of aquatic vegetation with conventional methods. Moreover, depending on survey of coarse temporal intervals and limited sampling points make it difficult to detect the seasonal and interannual variability of submerged and floating-leaved vegetation across the entire lake. Satellite remote sensing techniques have become powerful and effective tools for mapping aquatic vegetation types and for subsequent detection of changes in the vegetation types over a large area and a long time period. In recent decades, studies have been mapped aquatic vegetation in shallow coastal waters or lakes using optical remote sensing in many locations (Dogan et al., 2009; Laba et al., 2010; Peneva et al., 2008; Szantoi et al., 2013). Because of availability and accessibility, moderate spatial resolution multispectral satellite imagery, such as Landsat Multispectral Scanner (MSS), Thematic Mapper (TM) and Enhanced Thematic Mapper Plus (ETM+), have been

* Corresponding authors. Current address: 73 East Beijing Road, Nanjing, China. Tel.: +86 25 8688 2168; fax: +86 25 5771 4759.
E-mail addresses: jhluo@niglas.ac.cn (J. Luo), rhma@niglas.ac.cn (R. Ma).

http://dx.doi.org/10.1016/j.ecolind.2015.07.029
1470-160X/

used for mapping aquatic macrophytes (Ma et al., 2011; Pu et al., 2012; Zhao et al., 2012). Classification results from these moderate spatial resolution sensors have also been used to assess the interannual variability of aquatic vegetation effectively track and mitigate harmful changes especially in cases of eutrophication of shallow lakes, such as China's Taihu Lake (Zhao et al., 2012, 2013). However, there are few studies to monitoring seasonal changes or phenology of aquatic vegetation types using moderate spatial resolution remote sensing data. To better understand the wetland ecology process and effectively manage the lakes, it was worthwhile to monitor phenology of aquatic vegetation types and clarify time periods when cover area of different types reached their maxima. Unfortunately, acquiring successive dates of cloud-free TM images to monitor phenology of aquatic vegetation types proved difficult because of frequent overcast and rainy conditions in the Taihu Lake region. Huangjing Charge-Couple Device (HJ-CCD) images may be more appropriate than Landsat TM/ETM+ for monitoring phenology of aquatic vegetation types in Taihu Lake. The satellite sensor has a re-visit observation cycle of 48 h (two days) and spatial resolution of 30 m and was launched by the China Center for Resources Satellite Data and Application (CRESDA) in 2009.

Our objectives for this study were to (1) map aquatic vegetation types in Taihu Lake using HJ-CCD and Landsat TM images that were collected from 1984 to 2013, (2) examine the seasonal dynamics of different aquatic vegetation types and determine time periods when the areas covered by these vegetation types reached their maximum extents, and (3) assess the interannual changes of aquatic vegetation types from 1984 to 2013.

2. Materials and methods

2.1. Study area

Taihu Lake (30°55′40″–31°32′58″ N, 119°52′32″–120°36′10″ E) is one of the five largest freshwater lakes in China. Covering an area of about 2338 km^2. It is located at the core of the Yangtze Delta in the lower reaches of the Yangtze River in eastern China (Fig. 1). It is a typical shallow lake with a maximum depth of less than 3 m and an average depth of 1.9 m.

Taihu Lake can be divided into an algae-type zone (algal-dominated) and a grass-type zone (grass-dominated) (Fig. 1). The borders of the algae and grass-type zones have been generalized from past field observations of the spatial distribution of aquatic vegetation and the occurrence algae over the years. Algal blooms occur frequently in the algae-type zone (Duan et al., 2009). In the grass-type zone, the lake bottom is covered with hydrophytes and the water quality is better than that in the algae-type zone (Xu et al., 2014). To describe seasonal changes of total nitrogen (TN), total phosphorus (TP) and Secchi depths (SD) in the algae and grass-type zones, we averaged these parameters in February, May, August and November from 2008 to 2010 (Table 1) (data provided by Taihu Laboratory for Lake Ecosystem Research). As shown in Table 1, the grass-type zone had much lower TN and TP content and higher water transparency than did the algae type zone across all seasons. There are four types of aquatic vegetation in the grass-type zone: (i) emergent species, which are rooted in the bottom substrate but extend above the water surface (they are mostly distributed in a littoral zone of Taihu Lake); (ii) floating-leaved hydrophytes, which

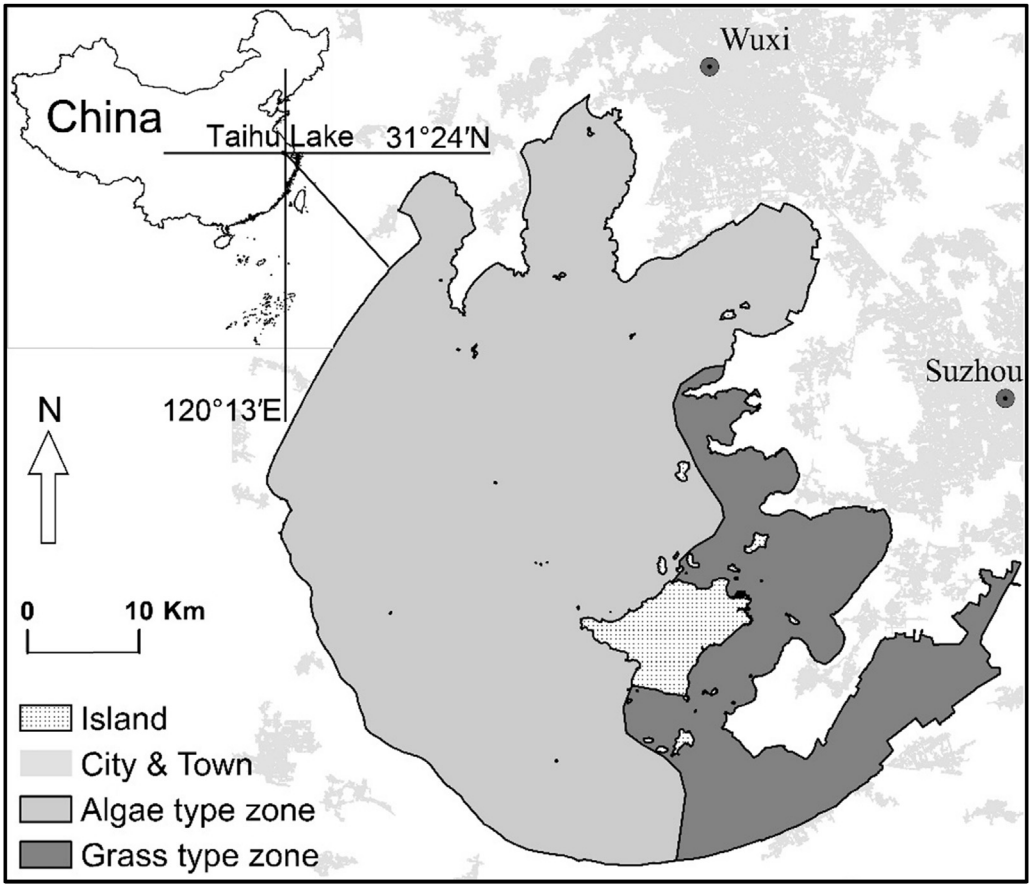

Fig. 1. Location of Taihu Lake within China and subarea of Taihu Lake.

Table 1
Total nitrogen (TN), total phosphorus (TP) and Secchi depths (SD) of the algae-type and grass-type zone from 2008 to 2010 (data from Taihu Laboratory for Lake Ecosystem Research).

	Algae-type zone			Grass-type zone		
	TN (mg/L)	TP (mg/L)	SD (m)	TN (mg/L)	TP (mg/L)	SD (m)
February	4.27 ± 2.32	0.11 ± 0.03	0.27 ± 0.04	1.70 ± 0.29	0.08 ± 0.03	0.45 ± 0.07
May	4.22 ± 0.91	0.10 ± 0.06	0.28 ± 0.05	2.16 ± 0.36	0.05 ± 0.02	0.52 ± 0.04
August	1.90 ± 0.40	0.09 ± 0.06	0.56 ± 0.06	1.03 ± 0.15	0.06 ± 0.04	1.04 ± 0.08
November	2.37 ± 0.38	0.13 ± 0.01	0.42 ± 0.05	1.50 ± 0.80	0.08 ± 0.03	0.78 ± 0.05

Table 2
Aquatic vegetation types and dominant species in the grass-type zone of Taihu Lake.

	Type	Dominant species
Type I	Emergent vegetation	*Phragmites communis, Zizania latifolia*
	Floating-leaved vegetation	*Eichhornia crassipes, Lemna minor, Nymphoides peltata, Trapa bicornis*
Type II	Submerged vegetation	*Vallisneria spiralis, Ceratophyllum demersum, Potamogeton malaianus, P. maackianus, Hydrilla varticillata*

are rooted in the sediment but have leaves floating on the water surface; (iii) free-floating hydrophytes, which float on the water surface with roots free of the bottom substrate (these plants move freely with wind and with water currents); and (iv) submerged hydrophytes, which are usually rooted in the bottom substrate with their foliage normally underwater.

Our study area focuses on only the grass-type zone. The dominant species in Taihu Lake are listed in Table 2. Aquatic vegetation in the grass-type zone can be divided into two types according to whether leaves are above (Type I) or below (Type II) the water's surface. The Type I vegetation includes emergent, floating-leaved and free-floating species, while Type II is comprised of submerged species.

2.2. Field data collection

Field surveys were carried out from September 20 to 23, 2002, July 10 to 13, 2013 and September 23 to 26, 2013. A total of 441 ground samples, including 150 samples from September 2002, 112 samples from July 2013 and 179 samples from September 2013, were collected from open water and aquatic vegetation types in the grass-type zone of Taihu Lake. The sampling plots were limited to the areas where aquatic vegetation was uniformly distributed over an extent at least 60 m × 60 m (i.e., four pixels of one HJ-CCD image). At each sampling plot, the type and coverage of aquatic vegetation were estimated by visual observation, and location coordinates were recorded from the plot center using a portable GPS receiver from the Trimble Geoexplorer 6000 series with an accuracy of less than 3 m.

2.3. Remote sensing data collections and processing

HJ-CCD images recorded from HJ-1A/1B CCD cameras were acquired from the China Center for Resources Satellite Data and Application (CRESDA). These cameras were onboard the HJ-1A and HJ-1B satellites which were launched by China Center for CRESDA on September 6, 2008. Their spectral ranges and spatial resolutions are similar to those of the first four bands of Landsat TM. A single CCD imagery width is 360 km, and the two satellites constellation provides a wider swath width (700 km) and a re-visit observation cycle of 48 h (two days). Its high re-visit cycle and wide swath width coverage are considered to be of great importance for vegetation monitoring and observation, especially during wet summers (i.e., between June and September) in southern and eastern China. In this study, 73 cloud-free HJ-CCD images without sun glint effect and covering Taihu Lake were acquired from January 2009 through December 2013 to study the seasonal dynamics of aquatic vegetation types (Table 3). In addition, we also acquired 7 cloud-free Landsat 5 TM images covering the study area that had been collected during August and September since 1984 for detecting interannual variation of aquatic vegetation types (Table 3).

Pre-processing of remote sensing images was conducted using ENVI software. Radiometric corrections were made using coefficients from the metadata accompanying the images (e.g., gains and offsets). The FLAASH module in the ENVI software was applied for atmospheric correction. Four key input parameters for the FLAASH module included: the mid-latitude atmosphere model, urban aerosol model, atmosphere water vapor and visibility. Based on the location of the study area covered by the scenes and satellite transit time, the first two parameters were easily determined. However, water vapor and visibility values may vary with images, and these were determined by trial-and-error until a typical spectral pattern of plants was observed. HJ-CCD and TM images were also geometrically corrected with a previously corrected Landsat TM image with a geometric accuracy of <0.5 pixel.

2.4. Meteorological data

The influence of air temperature on aquatic vegetation in Taihu Lake was also considered. The daily mean air temperature data at the Dongshan station in Taihu from January 2009 to December 2013 were acquired from the China Meteorological Data Sharing Service.

Table 3
Dates of HJ-1A/B and Landsat TM images.

Sensors	Years	Date of image
HJ-1A/B	2009	1/16, 2/12,3/14, 4/21, 5/1, 5/22, 6/25, 7/20, 8/28, 9/10, 10/2, 10/15, 10/31, 11/4, 11/23, 12/19, 12/26
	2010	2/21, 3/12, 4/7, 4/30, 5/12, 5/25, 6/6, 6/19, 7/31, 8/13, 9/8, 9/18, 10/31, 11/9, 12/7, 12/20
	2011	1/31, 3/7, 3/28, 4/25, 4/29, 5/13, 7/30, 9/24, 10/9, 11/12, 11/26, 12/12
	2012	1/7, 1/23, 2/4, 3/13, 3/25, 4/23, 5/6, 5/17, 7/21, 8/18, 9/2, 9/19, 10/10, 10/23, 11/7, 11/27, 12/12, 12/31
	2013	1/18, 2/20, 3/12, 4/25, 5/22, 7/11, 8/16, 9/26, 10/28, 11/17
Landsat 5 TM	8/4/1984, 8/7/1985, 9/14/1990, 8/29/1993, 8/11/1998, 8/3/2001, 9/12/2004	

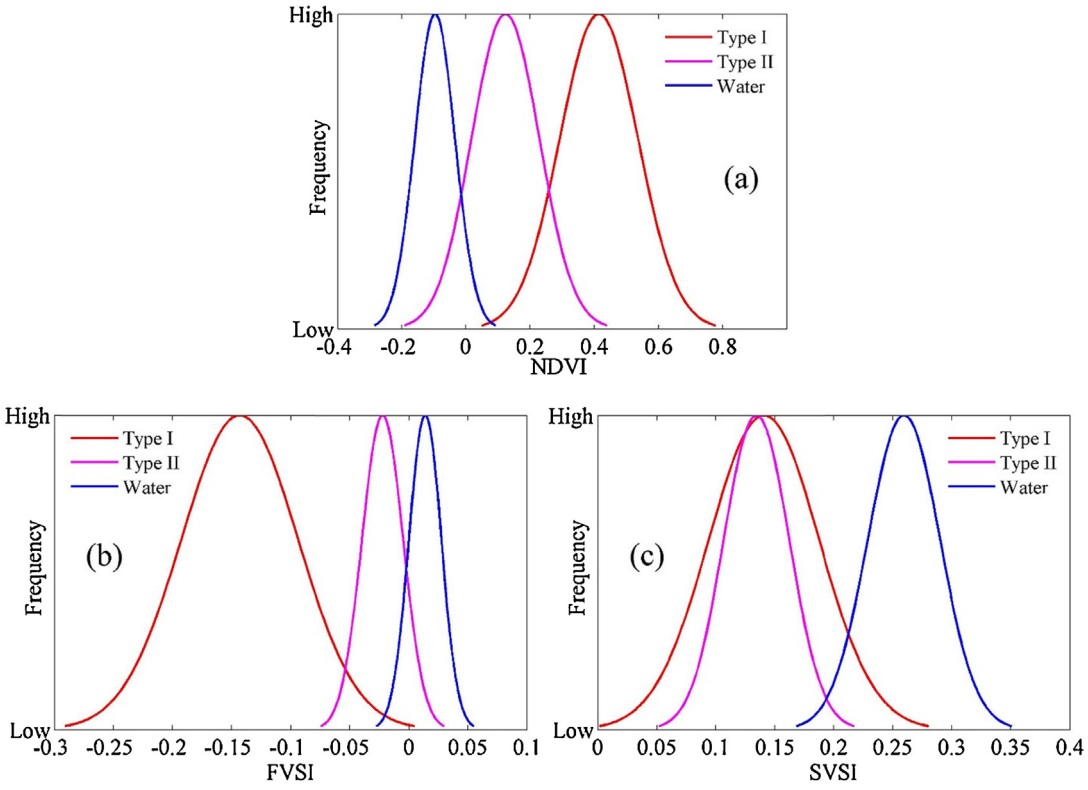

Fig. 2. Separability of Type I, Type II and water with NDVI (a), FVSI (b) and SVSI (c) derived from the image acquired on September 26, 2013.

The synchronous temperature ($\bar{T}_m$) with an image was calculated by:

$$\bar{T}_m = \frac{\sum_n^m T_i}{(m-n)} \quad (1)$$

where n is a focus image date; m is date after the focus image date; T_i is the daily mean temperature ($i = n, \ldots, m$) and $\bar{T}_m$ is the average of temperature from date n to date m with an interval of one day.

2.5. Water quality data

Water quality data, including the concentration of total nitrogen (TN) and total phosphorus (TP), were collected from the grass-type zone in mid-August from 1992 to 2013. These data were provided by the Taihu Laboratory for Lake Ecosystem Research. The dataset was used to test the hypothesis that the change in a simple ratio of Type II area to Type I area (abbreviated as $S_{Type\text{-}II}/S_{Type\text{-}I}$) is a good indicator of changes in the eutrophication and stable state of an aquatic system.

2.6. Methods

2.6.1. Classification tree (CT) model

A classification tree (CT) analysis is based on dichotomous partitioning of data at certain thresholds of the explanatory variables' value, which determine the branch a particular sample will follow (Olshen and Stone, 1984), and is considered to be especially robust when used with a small sample size of remotely-sensed data (Tadjudin and Landgrebe, 1996). Generally speaking, normalized differential vegetation index (NDVI) or even single band such as the near-infrared (NIR) band, is enough to distinguish between the vegetation and water. However, taking the image acquired on September 26, 2013 as an example, Fig. 2a shows that NDVI ranges of Type I, Type II and water had large overlap areas due to high suspension and low transparency in study area, which resulted in large misclassification error between these types. Luo et al. (2014) showed that the second principal component (PC_2) after the principal component transformation is sensitive to the floating-leaved vegetation. The eigenvector matrix shows that the infrared band had the highest contribution to the PC_2 with the coefficient equaled to 0.7688 (Table 4). Compared with Type II and water, Type I has the highest reflectance value in the near-infrared region because of its leaves above the water, which explained why PC_2 performed well on identifying Type I. Here, PC_2, named as floating-leaved vegetation sensitive index (FVSI) (Eq. (2)). Fig. 2b shows that there was a small overlap area between FVSI range of Type I and other two types, and FVSI perform better than NDVI in exactly extracting Type I from other types. Meanwhile, a submerged vegetation sensitive index (SVSI) (Eq. (3)) was also developed by combining brightness with greenness derived from tasseled cap transform. Fig. 2c shows that there was a small overlap area between SVSI range of Type II and water, so SVSI had the most potential in distinguishing Type II and water. Therefore, a classification tree with FVSI and SVSI as classification features of nodes was developed. As shown in Fig. 3, Type I was first exacted from other types using FVSI, and then SVSI was used to distinguish between Type II from water. The

Table 4
Eigenvectors of variance-covariance matrix in the September 26, 2013 image.

Band	PC_1	PC_2	PC_3	PC_4
Blue band	0.4247	0.5280	0.4397	0.5510
Green band	0.3089	0.3702	0.2685	−0.8339
Red band	−0.5154	−0.2081	0.8256	−0.0264
Infrared band	−0.6771	0.7688	−0.2302	−0.0147

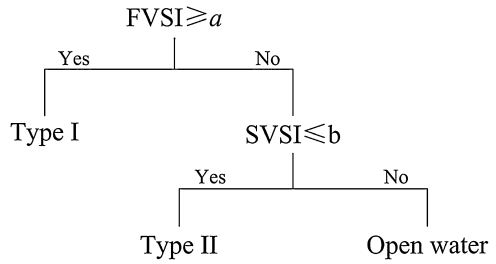

Fig. 3. Classification tree model structures for Types I and Type II. *a* and *b* are the thresholds of FVSI and SVSI, respectively, and the thresholds varied with each image.

thresholds of FVSI and SVSI varies with images. The FVSI and SVSI were defined as:

$$\mathrm{FVSI} = \mathrm{PC}_2 \tag{2}$$

where PC_2 is the second principal component of the principal component transform:

$$\mathrm{SVSI} = \mathrm{TC}_1 - \mathrm{TC}_2 \tag{3}$$

where TC_1 and TC_2 are, respectively, the first and the second components of the tasseled cap transform, namely also brightness and greenness (Crist, 1985; Healey et al., 2005).

2.6.2. Method for determining the thresholds

For the image with synchronously collected ground samples, the thresholds of FVSI and SVSI were determined and modified slightly based on field survey points until the maximum classification precision was achieved. And for the image in the absence of synchronously collected ground samples, how can we determine the corresponding thresholds, especially for the historical distribution of aquatic vegetation in a shallow lake? Luo et al. (2014) developed an effective algorithm to calculate the thresholds for the CT model for the image in the absence of corresponding ground samples.

In this study, we used the algorithm developed by Luo et al. (2014) to calculate the thresholds of FVSI and SVSI in CT models for historical images acquired at any time without synchronously collected ground samples. The algorithms can be expressed as:

$$\mathrm{CT}_m\_\mathrm{FVSI} = k \times \mathrm{CT}_n\_\mathrm{FVSI} + h \tag{4}$$

$$\mathrm{CT}_m\_\mathrm{SVSI} = p \times \mathrm{CT}_n\_\mathrm{SVSI} + q \tag{5}$$

where CT_m_FVSI and CT_m_SVSI are the thresholds of FVSI and SVSI in the classification model for the image acquired at time m in the absence of ground samples, which should be calculated; CT_n_FVSI and CT_n_SVSI are the thresholds of FVSI and SVSI in the classification model for the image acquired at time n with synchronously collected ground samples, and the CT_n_FVSI and CT_n_SVSI were obtained based on the field survey data. As for *k* and *h*, we firstly selected same region of interests (ROIs) with Type I from images at time *m* and *n*, respectively. Secondly, two group FVSI values derived from two ROIs were descending order. Finally, the line fitting model was simulated by using two descending FVSI datasets, and the slope and intercept of the line model was k and h, respectively. In a similar way, the line fitting model could be simulated by the two groups of SVSI in descending order, and then we can acquire *p* and *q*. See the work by Luo et al. (2014) for the detailed test and validation of the algorithm.

The thresholds and classification accuracies were assessed by within classification accuracy (WCA) and overall classification accuracy (OCA) (Gao and Xu, 2015) that were calculated as follows:

$$\mathrm{WCA}_i = \frac{P_i}{M_i} \times 100\% \tag{6}$$

$$\mathrm{OCA} = \frac{\sum_{i=1}^{C} P_i}{P} \times 100\% \tag{7}$$

In these equations, P_i denotes the number of correctly classified samples in *i*th class, M_i is the total samples in *i*th class; *C* is the number of classes, while *P* is the total number of samples in the test dataset.

2.6.3. Analyzing seasonal change

Field measurements have shown that the logistic model is effective for depicting vegetation growth curves as a function of time (Beck et al., 2006). The double logistic model has been used to monitor land surface phenology in previous studies, and is adequate for most of the biomes present globally (Beck et al., 2006; Julien and Sobrino, 2009). Recent analyses from Li et al. (2011) and Hird and McDermid (2009) suggested that a double logistic function could more accurately describe the duration of the growing season and optimally reduce noise in remote sensing time series. In this study, we attempted to obtain the seasonal changes of Type I and Type II using the double logistic fitting function.

3. Results

3.1. Identification of aquatic vegetation

We determined the thresholds of FVSI and SVSI, and developed a CT model based on July 11, 2013 image and 179 synchronously collected ground samples. The CT model had an overall accuracy of 88.5%, with classification accuracies of 92.7% and 82.5% for Type I and Type II, respectively. Among misclassified samples, 83% were floating-leaved and submerged vegetation with a coverage of <20%, which were misclassified as open water. The classification results suggested that it might be difficult to identify submerged and floating-leaved vegetation with a coverage of <20% using satellite images with a resolution of 30 m (e.g., HJ-CCD and TM images). In this study, the CT model with appropriate thresholds of FVSI and SVSI could be used to correctly identify the submerged vegetation with a coverage of >20%.

Next, based on the threshold of FVSI and SVSI for July 11, 2013, we calculated the all thresholds of FVSI and SVSI for all images using the algorithms (Eqs. (2) and (3)). Table 5 lists the thresholds of FVSI and SVSI for several images and corresponding classification accuracies. In Table 5, the thresholds for September 23, 2002 and September 26, 2013 were calculated based on the thresholds of the CT model for July 11, 2013, and OCAs of classification were higher than 75%. The result indicated that we could obtain historical distribution maps of Type I and Type II with historical remote sensing images in the absence of corresponding ground samples using the algorithms (i.e., Eqs. (4) and (5)).

3.2. Seasonal dynamics of aquatic vegetation

The CT models were used to map Type I and Type II in the grass-type zone of Taihu Lake, and a total of 73 classification maps for the period from January 16, 2009 to November 17, 2013 were produced. For each classification map, the areas covered by Type I and

Table 5
Thresholds and classification accuracies of CT models. See Fig. 3 for description of classification tree; *a* and *b* are the thresholds of FVSI and SVSI, respectively.

Sensors	Date	Thresholds		WCA (%)		OCA (%)
		a	*b*	Type I	Type II	
HJ-CCD	07/11/2013	2.17	0.19	83.6	80.1	82.1
	09/26/2013	1.63	0.18	84.82	81.82	75.5
Landsat TM	9/23/2002	2.17	0.09	85.4	82.2	75.6

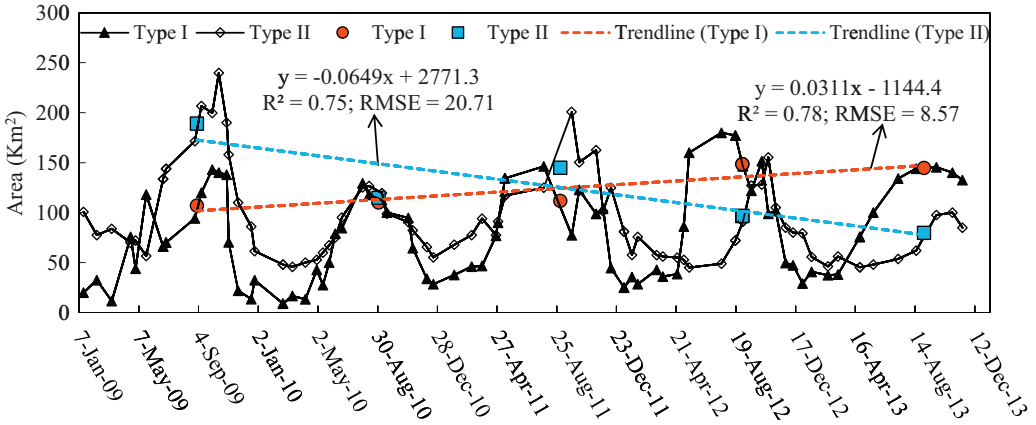

Fig. 4. Dynamics of the distribution area and change trend of aquatic vegetation from 2009 to 2013. The red and blue dots represent yearly areas of Type I and Type II, individually; the red and blue trend lines represent change trend of Type I and Type II. (For interpretation of the references to color in this figure legend, the reader is referred to the web version of this article.)

Type II were calculated. In order to describe the interannual area change trends of Types I and Type II over the five-year period, we averaged vegetation areas of Types I and Type II, individually, from August to September every year. The fitting lines between yearly areas and corresponding years were used to describe the interannual change tendency of aquatic vegetation types, and the effects of the fitting model were assessed via R^2 and RMSE. A positive slope of the fitting model indicated an increasing trend, and a negative slope indicated a decreasing trend over the period. As shown in Fig. 4, the area of Type I had a tiny increasing trend whereas there was a slowly decreasing trend for Type II over the past five-year period. In Fig. 4, unsystematic area variations in the growth periods of vegetation might be induced by many factors, such as vegetation harvesting, classification error, and difference of growth period among different dominant species.

Cover areas of Type I and Type II derived from 73 HJ-CCD images from 2009 to 2013 were reconstituted as a year dataset to describe their seasonal dynamics (Fig. 5). We used areas of Type I and Type II to model their growing season phenology by logistic functions. From Fig. 5, the areas of Type I and Type II first increased and then decreased, which conformed to the double logistic curve. But the details of the growing season phenology were different. For Type I, a growth season onset and end occurred in mid-March (DOY = 70) and mid-December (DOY = 350). Yet in mid-July (DOY = 194) and

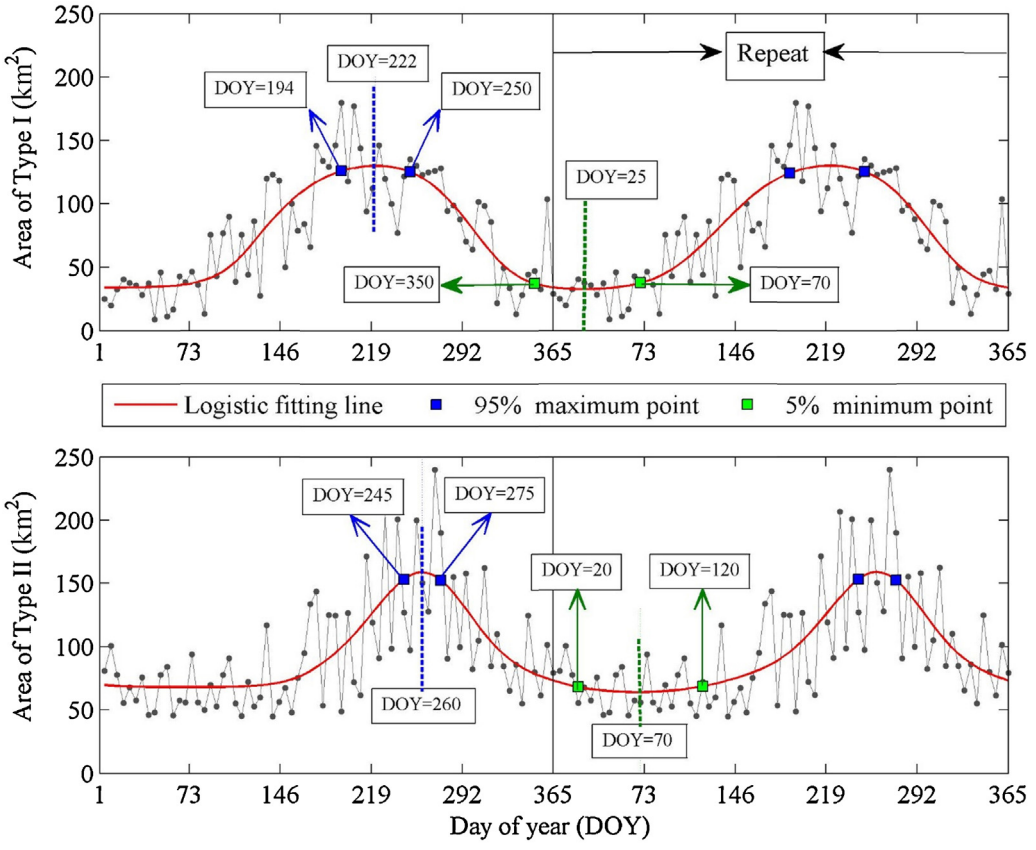

Fig. 5. Seasonal changes of Type I and Type II with logistic fitting lines.

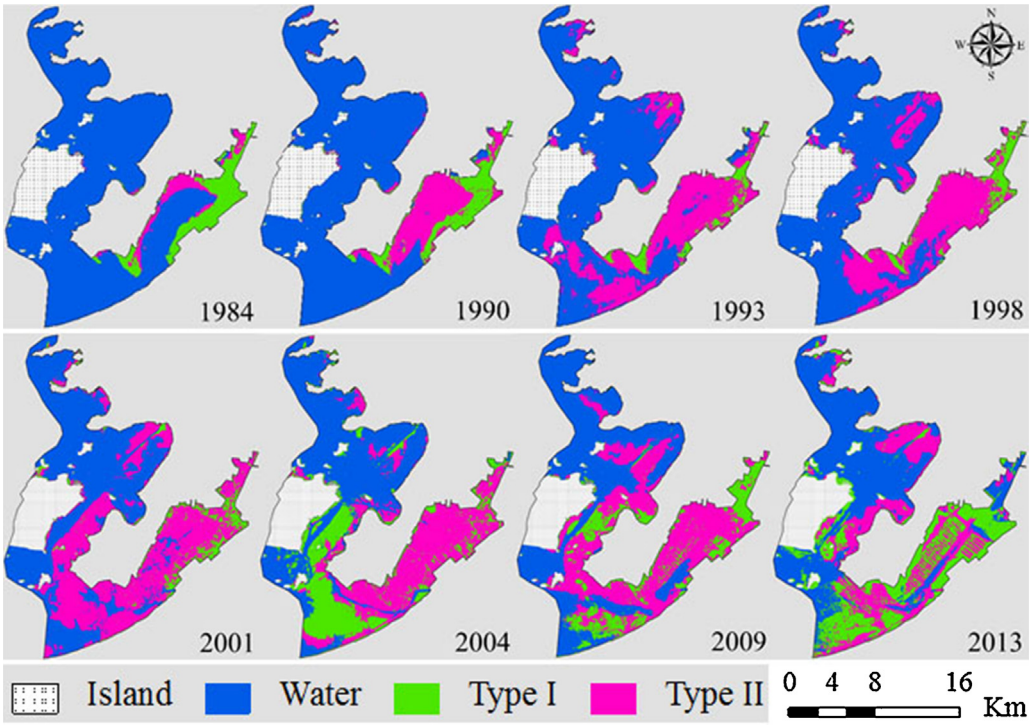

Fig. 6. Spatial distributions of Type I and Type II from 1984 to 2013 in the grass-type zone of Taihu Lake. Type I vegetation consists of emergent, floating-leaved and free-floating vegetation, whereas Type II consists of submerged vegetation.

early September (DOY = 250), the Type I reached its top values for the whole growing period. The peak of the area as estimated by the logistic fitting model occurred in the middle of August (DOY = 222). For Type II, a dormant season onset and end occurred in mid-January (DOY = 20) and at the end of April (DOY = 120), respectively. The peaks of Type II occurred early September (DOY = 245) and early October (DOY = 275) over the whole growing period. According to the logistic fitting model, the area peak occurred in mid-September (DOY = 260), which lagged behind Type I.

3.3. Interannual variation of aquatic vegetation

The spatial distribution of Type I and Type II in the grass-type zone (in the eastern part of Taihu Lake) was mapped from 1984 to 2013 (Fig. 6) using Landsat 5 TM and HJ-CCD images obtained between early August and mid-September (when the area of aquatic vegetation was at the maximum according to the results described above). Over this period, the spatial distribution of aquatic vegetation experienced some changes near the northern and eastern shores of the lake, and the distribution of Type I significantly increased, especially in the southern part.

Fig. 7 illustrated the interannual dynamics of the distribution areas of Type I, Type II and total aquatic vegetation (Type I + Type II) from 1984 to 2013. Substantial changes were observed in the distribution areas of Type I and Type II as well as the total aquatic vegetation. The area covered by Type I showed a continuous increase from 59.75 km^2 (1984) to 148.00 km^2 (2013) (R^2 = 0.84, RMSE = 14.16); the area covered by Type II first increased and then decreased with the changes conforming to a significant quadratic curve (R^2 = 0.83, RMSE = 22.36), and with the maximum area occurring roughly in 2000. The total area of aquatic vegetation increased significantly from 87.84 km^2 (1984) to 297.68 km^2 (2004) and then decreased slightly to 224.55 km^2 (2013) (R^2 = 0.90, RMSE = 23.5). The maximum area in the grass-type zone occurred around 2005.

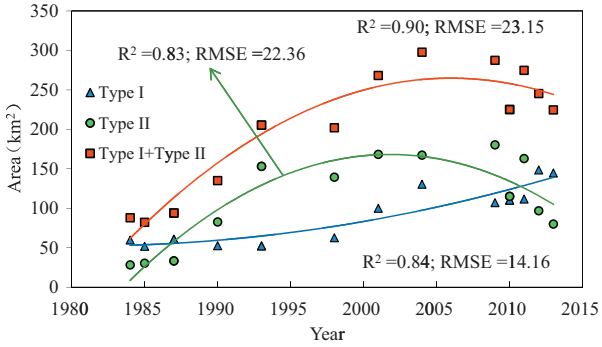

Fig. 7. Temporal trends (1984–2013) of the distribution area of Type I and Type II as well as total aquatic vegetation.

4. Discussion

4.1. Response of aquatic vegetation to air temperature

A variety of environmental factors can interact directly affect the productivity, distribution, and species composition of aquatic plants. These factors include climatic factors (such as temperature, wind and precipitation), light availability and characteristics inherent in the limnology of water bodies (sediment composition, water transparency, nutrients and trophic status, etc.) (Barko et al., 1986, 1991; Carpenter and Lodge, 1986). Of these, the ambient temperature is one of the most important factors that influence aquatic plants (Barko et al., 1982); no other individual factors have a more profound direct and indirect influence on the physicochemical, biological, metabolic and physiological behaviors of aquatic ecosystems than does temperature (Carr et al., 1997), especially water temperature. Water temperature can directly affect submerged vegetation growth. Unfortunately, continuous measured

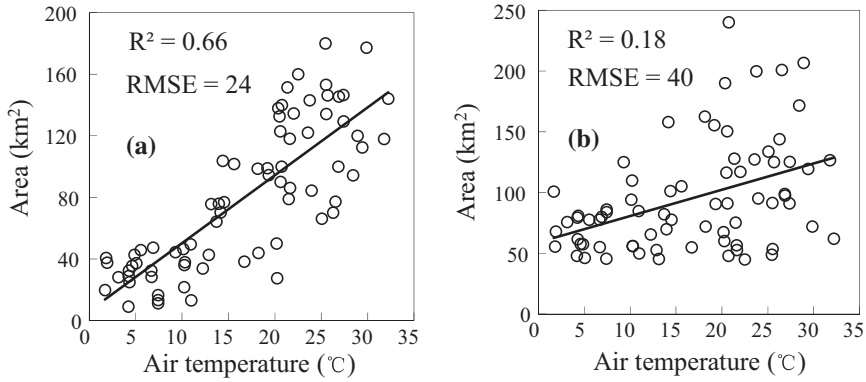

Fig. 8. Correlation analyses between the distribution areas of Type I (a) and Type II (b) and air temperature.

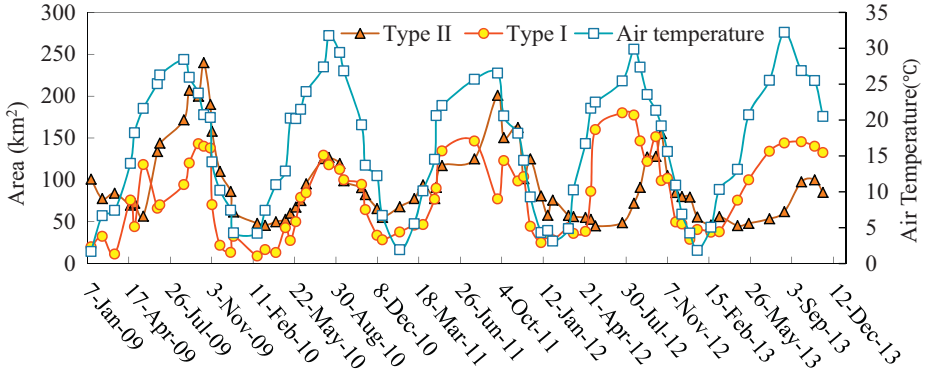

Fig. 9. Dynamic changes in Type I and Type II areas as well as air temperature.

water temperature data were not available for this study. Instead, we would use measured air temperature data only to do correlation analysis with vegetation area.

There was a significant positive correlation between Type I and air temperature (R^2 = 0.66, RMSE = 27) (Fig. 8a), while for Type II the corresponding correlation coefficient was pretty low with air temperature (R^2 = 0.18, RMSE = 40) (Fig. 8b). In addition, Fig. 9 also illustrates the dynamic changes in the air temperature and the area of Type II over the time from January 2009 to December 2013, and their changes in these variables were not synchronous. Possible explanations for the above results may include: (i) Type I vegetation has a large portion of their leaf surface exposed to the atmosphere, which increases interaction chance with air temperature; and (ii) the foliage of Type II vegetation is normally underwater, so that the growth of Type II vegetation should be more influenced by the water temperature than by the air temperature. The change in water temperature is usually slower than in air temperature because water has a higher heat capacity (Denny, 1993).

Fig. 9 demonstrates that the curves of the distribution area of Type II were consistent with the air temperature curve if the air temperature curve was moved left one month. Fig. 10 presents a relationship between the area of Type II and the air temperature recorded one month before. Such a shift produced a marked improvement in coefficient of determination (R^2) from 0.18 to 0.42. The result suggested that air temperature had a lag effect on the growth of Type II, which explained why the times of maximum areas of Type II lagged 38 days behind Type I (Fig. 5). Additionally, there appeared to increase variance with increasing temperature in the Type II as seen in Fig. 8b and Fig. 10. It is possible that the air temperature is a dominant factor in the growth of submerged vegetation at low temperature (T < 18 °C, from April to November). When T > 18 °C, temperature might be not a limiting factor of submerged vegetation, while other factors, such as nutrient variables, water transparency and water depth, may have a greater effect on submerged vegetation than air temperature(Dong et al., 2014).

4.2. Stable state of Taihu Lake from aquatic vegetation change

A stable state of an aquatic system could be related to its aquatic vegetation composition. Scheffer et al. (2003) proposed a stable state theory of freshwater ecosystems based on their experiments, field data and modeling, and found that nutrient enrichment might reduce the resilience of freshwater systems and should shift the

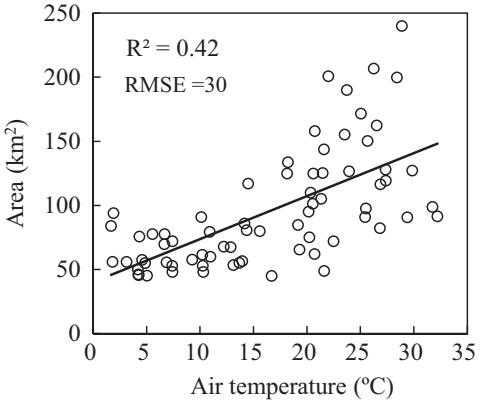

Fig. 10. Correlation between the area of Type II and the air temperature a month ago.

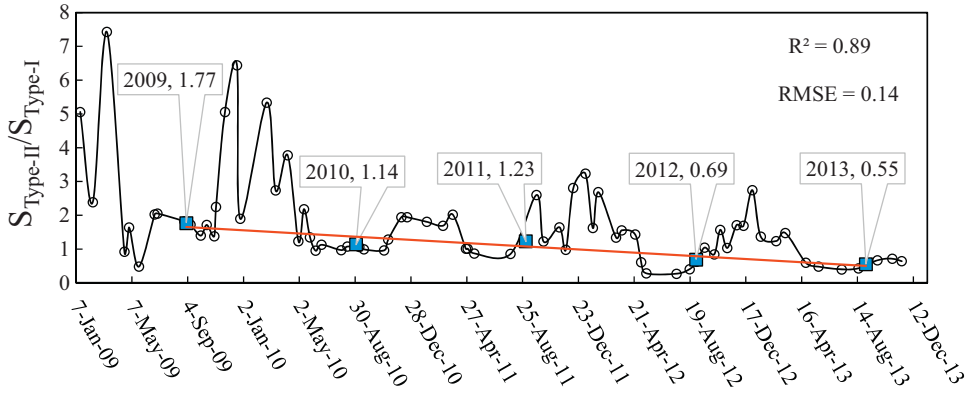

Fig. 11. Changes in $S_{Type\text{-}II}/S_{Type\text{-}I}$ from 2009 to 2013.

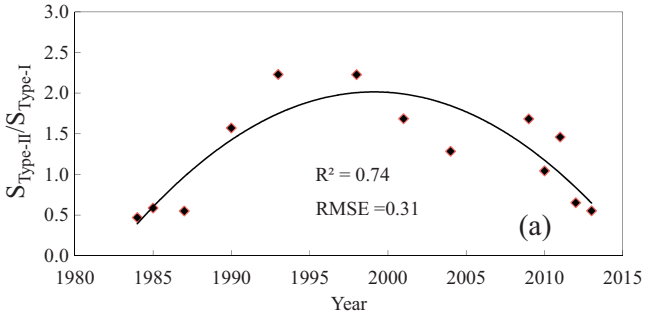

Fig. 12. Changes in the $S_{Type\text{-}II}/S_{Type\text{-}I}$ from 1984 to 2013.

aquatic vegetation toward dominance by floating plants. Egertson et al. (2004) also found that the eutrophication of shallow lakes often leads to a shift in the macrophyte community from dominance by submerged vegetation to dominance by floating-leaved plants. Therefore, the change in the $S_{Type\text{-}II}/S_{Type\text{-}I}$ over time seemed to be a good indicator of changes in the eutrophication and stable state of an aquatic system. According to Fig. 5, the maximum area of aquatic vegetation appeared in the period across August and September, and therefore we separately averaged the areas for Type I and Type II from August to September every year as corresponding yearly areas; we then calculated yearly $S_{Type\text{-}II}/S_{Type\text{-}I}$ value from 2009 to 2013. The corresponding change trend line might be obtained by fitting the relationship between the $S_{Type\text{-}II}/S_{Type\text{-}I}$ and year, and the change trend was assessed by R^2 and RSME values. As shown in Fig. 11, the change trend of the $S_{Type\text{-}II}/S_{Type\text{-}I}$ in Taihu Lake from 2009 to 2013 was slowly decreasing, with a rate of change of 0.31% per year.

Similar to Fig. 11, we obtained the change in the $S_{Type\text{-}II}/S_{Type\text{-}I}$ from 1984 to 2013 (Fig. 12). The result in Fig. 12 shows that the $S_{Type\text{-}II}/S_{Type\text{-}I}$ first increased and then decreased with the changes conforming to the shape of a significant quadratic curve ($R^2 = 0.74$, RMSE = 0.31). The turning point seemed to be located in about 2000. This is an adverse signal for the grass-type zone of Taihu Lake; it suggests that water quality and eutrophication of Taihu Lake would have not been improved and, in fact, have been getting worse since 2000. Fig. 13 shows that the change trends in concentration of TN and TP from 1992 to 2013 were opposite with the $S_{Type\text{-}II}/S_{Type\text{-}I}$, which validated the hypothesis above. The result indicated that their change tendency is the opposite with the $S_{Type\text{-}II}/S_{Type\text{-}I}$, which validate above hypothesis to some extent.

4.3. Applications and management

In shallow lakes, aquatic macrophytes are primary producers and play important roles in maintaining the balance of lake ecosystems. Existing research has shown that aquatic vegetation has a significant and positive effect on nutrient pollutant removal and thereby purifies water (Iamchaturapatr et al., 2007; Tang et al., 2009). However, an excessive amount of macrophytes, especially floating-leaved vegetation, can cause silting through the addition of large amounts of plant material to lake bottom and release pollutants into the lake water when the plants die and decay (Vereecken et al., 2006), even resulting in shifting from grass-type lakes to algae-type lakes. As for eutrophic Taihu Lake, due to high nutrient content, the excessive growth of aquatic plants frequently occurred. Moderate harvesting of aquatic vegetation, especially for Type I,

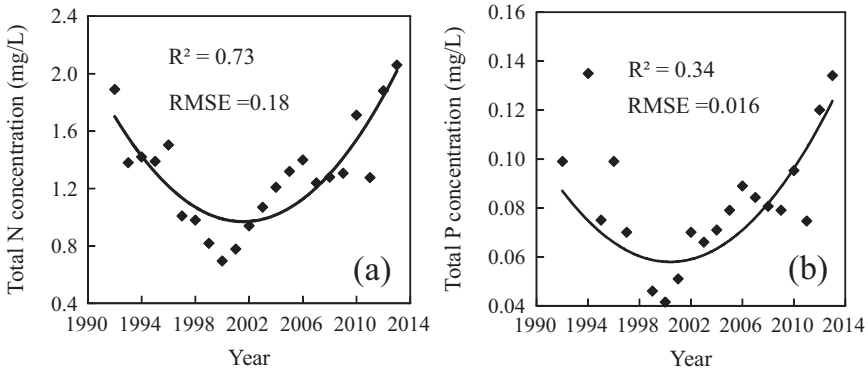

Fig. 13. Changes in concentration of TN and TP from 1992 to 2013.

could prevent from swamping to some extent (Reisinger et al., 2008; Vereecken et al., 2006; Vymazal et al., 2010). Our results indicated that harvest engineering might be conducted from mid-July to early September for Type I and in September for Type II (Fig. 5). Analysis of the changes in $S_{Type\text{-}II}/S_{Type\text{-}I}$ from 1984 to 2013 shows that the $S_{Type\text{-}II}/S_{Type\text{-}I}$ has been declining continuously but slowly, which suggests that the management department should take measures to prevent the aquatic systems from shifting from being dominated by submerged vegetation to being dominated by floating-leaved plants. For example, the most important measures may be to reduce pollutant and nutrient intake, meanwhile, harvesting Type I or artificially planting Type II is also an essential management methods.

Finally, our results also demonstrate a need for choosing a right remote sensing image to map both Type I and Type II. It is also important to study the spatio-temporal variability in Taihu Lake over a 20- to 30-year period. In this study, we did not adequately consider responses of wetland vegetation to regional climate, which would be helpful to understand the balance of aquatic vegetation over a long term (Euliss et al., 2004).

5. Conclusion

We used classification trees with FVSI and SVSI as classification features of the nodes to map aquatic vegetation (Types I and Type II) in Taihu Lake in this study. Based on 73 HJ-CCD images acquired from 2009 to 2013 and 7 Landsat TM images from 1984 to 2004, seasonal and interannual changes of Type I and Type II in Taihu Lake were analyzed.

The experimental results demonstrated that seasonal change patterns of Type I and Type II could be precisely described by the double logistic functions. According to logistic fitting models, the area of Type I reached its peak in mid-August; for Type II, the maximum area occurred in mid-September. The time of Type II reached maximum area lagged behind that of Type I, which could be attributable to air temperature. Air temperature was a key factor of aquatic vegetation growth and had a more direct effect on Type I ($R^2 = 0.66$) than Type II ($R^2 = 0.18$). From 1984 to 2013, in the grass-type zone, the $S_{Type\text{-}II}/S_{Type\text{-}I}$ first increased before 2000 and then decreased, which suggested that the aquatic system was shifting from being dominated by submerged vegetation to being dominated by floating-leaved plants.

Acknowledgments

The research was supported by National Natural Science Foundation of China (No. 41301375) and the State Key Program of National Natural Science Foundation of China (No. 41230853). We thank the Taihu Laboratory for Lake Ecosystem Research (TLLER) for providing water quality data. We also appreciate Scientific Data Sharing Platform for Lake and Watershed for providing remote sensing data (http://lake.geodata.cn), Nanjing Institute of Geography and Limnology, Chinese Academy of Sciences.

References

Barko, J., Adams, M., Clesceri, N., 1986. Environmental factors and their consideration in the management of submersed aquatic vegetation: a review. J. Aquat. Plant Manage. 24, 1–10.

Barko, J., Hardin, D., Matthews, M., 1982. Growth and morphology of submersed freshwater macrophytes in relation to light and temperature. C. J. Bot. 60, 877–887.

Barko, J.W., Gunnison, D., Carpenter, S.R., 1991. Sediment interactions with submersed macrophyte growth and community dynamics. Aquat. Bot. 41, 41–65.

Beck, P.S.A., Atzberger, C., Hogda, K.A., Johansen, B., Skidmore, A.K., 2006. Improved monitoring of vegetation dynamics at very high latitudes: a new method using MODIS NDVI. Rem. Sens. Environ. 100, 321–334.

Carpenter, S.R., Lodge, D.M., 1986. Effects of submersed macrophytes on ecosystem processes. Aquat. Bot. 26, 341–370.

Carr, G.M., Duthie, H.C., Taylor, W.D., 1997. Models of aquatic plant productivity: a review of the factors that influence growth. Aquat. Bot. 59, 195–215.

Crist, E.P., 1985. A TM tasseled cap equivalent transformation for reflectance factor data. Rem. Sens. Environ. 17, 301–306.

Denny, M.W., 1993. Air and Water: The Biology and Physics of Life's Media. Princeton University Press.

Dogan, O.K., Akyurek, Z., Beklioglu, M., 2009. Identification and mapping of submerged plants in a shallow lake using quickbird satellite data. J. Environ. Manage. 90, 2138–2143.

Dong, B.L., Qin, B.Q., Gao, G., Cai, X.L., 2014. Submerged macrophyte communities and the controlling factors in large, shallow Lake Taihu (China): sediment distribution and water depth. J. Great Lakes Res. 40, 646–655.

Duan, H., Ma, R., Xu, X., Kong, F., Zhang, S., Kong, W., Hao, J., Shang, L., 2009. Two-decade reconstruction of algal blooms in China's Lake Taihu. Environ. Sci. Technol. 43, 3522–3528.

Egertson, C.J., Kopaska, J.A., Downing, J.A., 2004. A century of change in macrophyte abundance and composition in response to agricultural eutrophication. Hydrobiologia 524, 145–156.

Euliss, N.H., Labaugh, J.W., Fredrickson, L.H., Mushet, D.M., Laubhan, M.R.K., Swanson, G.A., Winter, T.C., Rosenberry, D.O., Nelson, R.D., 2004. The wetland continuum: a conceptual framework for interpreting biological studies. Wetlands 24, 448–458.

Folke, C., Carpenter, S., Walker, B., Scheffer, M., Elmqvist, T., Gunderson, L., Holling, C., 2004. Regime shifts, resilience, and biodiversity in ecosystem management. Annu. Rev. Ecol. Evol. Syst., 557–581.

Gao, J., Xu, L., 2015. An efficient method to solve the classification problem for remote sensing image. AEU-Int. J. Electron. Commun. 69, 198–205.

Gumbricht, T., 1993. Nutrient removal processes in freshwater submersed macrophyte systems. Ecol. Eng. 2, 1–30.

Healey, S.P., Cohen, W.B., Zhiqiang, Y., Krankina, O.N., 2005. Comparison of tasseled cap-based Landsat data structures for use in forest disturbance detection. Rem. Sens. Environ. 97, 301–310.

Hird, J.N., McDermid, G.J., 2009. Noise reduction of NDVI time series: an empirical comparison of selected techniques. Rem. Sens. Environ. 113, 248–258.

Hu, L., Hu, W., Deng, J., Li, Q., Gao, F., Zhu, J., Han, T., 2010. Nutrient removal in wetlands with different macrophyte structures in eastern Lake Taihu, China. Ecol. Eng. 36, 1725–1732.

Iamchaturapatr, J., Yi, S.W., Rhee, J.S., 2007. Nutrient removals by 21 aquatic plants for vertical free surface-flow (VFS) constructed wetland. Ecol. Eng. 29, 287–293.

Julien, Y., Sobrino, J.A., 2009. Global land surface phenology trends from GIMMS database. Int. J. Rem. Sens. 30, 3495–3513.

Laba, M., Blair, B., Downs, R., Monger, B., Philpot, W., Smith, S., Sullivan, P., Baveye, P.C., 2010. Use of textural measurements to map invasive wetland plants in the Hudson River National Estuarine Research Reserve with IKONOS satellite imagery. Rem. Sens. Environ. 114, 876–886.

Li, M., Wu, Z.F., Qin, L.J., Meng, X.J., 2011. Extracting vegetation phenology metrics in Changbai Mountains using an improved logistic model. Chin. Geogr. Sci. 21, 304–311.

Li, W., Yang, Q., 1995. Wetland utilization in Lake Taihu for fish farming and improvement of lake water quality. Ecol. Eng. 5, 107–121.

Luo, J.H., Ma, R.H., Duan, H.T., Hu, W.P., Zhu, J.G., Huang, W.J., Lin, C., 2014. A new method for modifying thresholds in the classification of tree models for mapping aquatic vegetation in Taihu Lake with satellite images. Rem. Sens.-Basel 6, 7442–7462.

Ma, R., Duan, H., Liu, Q., Loiselle, S.A., 2011. Approximate bottom contribution to remote sensing reflectance in Taihu Lake, China. J. Great Lakes Res. 37, 18–25.

Olshen, L.B.J.F.R., Stone, C.J., 1984. Classification and Regression Trees. Wadsworth International Group.

Peneva, E., Griffith, J.A., Carter, G.A., 2008. Seagrass mapping in the northern Gulf of Mexico using airborne hyperspectral imagery: a comparison of classification methods. J. Coast. Res. 25 (4), 850–856.

Pu, R., Bell, S., Meyer, C., Baggett, L., Zhao, Y., 2012. Mapping and assessing seagrass along the western coast of Florida using Landsat TM and EO-1 ALI/Hyperion imagery. Estuar. Coast. Shelf Sci. 115, 234–245.

Reisinger, D.L., Brabham, M., Schmidt, M.F., Victor, P.R., Schwartz, L., 2008. Methodology, evaluation, and feasibility study of total phosphorus removal management measures in Lake George and nearby lakes. Fla. Water Resour. Res. 60, 42–50.

Scheffer, M., Szabo, S., Gragnani, A., Van Nes, E.H., Rinaldi, S., Kautsky, N., Norberg, J., Roijackers, R.M., Franken, R.J., 2003. Floating plant dominance as a stable state. Proc. Natl. Acad. Sci. U.S.A. 100, 4040–4045.

Soana, E., Naldi, M., Bartoli, M., 2012. Effects of increasing organic matter loads on pore water features of vegetated (*Vallisneria spiralis* L.) and plant-free sediments. Ecol. Eng. 47, 141–145.

Szantoi, Z., Escobedo, F., Abd-Elrahman, A., Smith, S., Pearlstine, L., 2013. Analyzing fine-scale wetland composition using high resolution imagery and texture features. Int. J. Appl. Earth Obs. 23, 204–212.

Tadjudin, S., Landgrebe, D.A.,1996. A decision tree classifier design for high-dimensional data with limited training samples. In: Geoscience and Remote Sensing Symposium, 1996. IEEE IGARSS, pp. 790–792.

Tang, X., Huang, S., Scholz, M., Li, J., 2009. Nutrient removal in pilot-scale constructed wetlands treating eutrophic river water: assessment of plants, intermittent artificial aeration and polyhedron hollow polypropylene balls. Water Air Soil Poll. 197, 61–73.

Vereecken, H., Baetens, J., Viaene, P., Mostaert, F., Meire, P., 2006. Ecological management of aquatic plants: effects in lowland streams. In: Macrophytes in Aquatic Ecosystems: From Biology to Management. Springer, pp. 205–210.

Vymazal, J., Kröpfelová, L., Švehla, J., Štíchová, J., 2010. Can multiple harvest of aboveground biomass enhance removal of trace elements in constructed wetlands receiving municipal sewage? Ecol. Eng. 36, 939–945.
Xu, W., Hu, W., Deng, J., Zhu, J., Li, Q., 2014. Effects of harvest management of *Trapa bispinosa* on an aquatic macrophyte community and water quality in a eutrophic lake. Ecol. Eng. 64, 120–129.
Zhao, D., Jiang, H., Yang, T., Cai, Y., Xu, D., An, S., 2012. Remote sensing of aquatic vegetation distribution in Taihu Lake using an improved classification tree with modified thresholds. J. Environ. Manage. 95, 98–107.
Zhao, D., Lv, M., Jiang, H., Cai, Y., Xu, D., An, S., 2013. Spatio-temporal variability of aquatic vegetation in Taihu Lake over the past 30 years. PLOS ONE 8, e66365.